

FPMC2013-4409

A SIMULATION MODEL OF A HYDRAULIC BUCK CONVERTER BASED ON A MIXED TIME FREQUENCY DOMAIN ITERATION

Helmut Kogler

Institute of Machine Design and Hydraulic Drives
Johannes Kepler University
Altenberger Str. 69, 4040 Linz, Austria
helmut.kogler@jku.at

Rudolf Scheidl

Michael Ehrentraut
Institute of Machine Design and Hydraulic Drives
Johannes Kepler University
Altenberger Str. 69, 4040 Linz, Austria
rudolf.scheidl@jku.at

ABSTRACT

Digital hydraulics is an opportunity to realize simple, robust, cheap and energy efficient hydraulic drives. In such systems digital on/off valves are used instead of proportional valves. Moreover, in hydraulic switching converters the valves are actuated within a few milliseconds, which create sharp pressure changes and, in turn, significant wave propagation effects in the pipe system. For a proper design of digital hydraulic systems a sound understanding of these effects is required to achieve the desired behavior of the switching drive system. In such converters, like the buck-, boost or boost-buck-converter, the inductance is one crucial component. It is realized by a simple pipe mainly for cost reasons. Furthermore, switching converters contain some components with nonlinear characteristics, like valves or accumulators, which prevent a comprehensive analysis in frequency domain. For a convenient analysis a qualified model of a hydraulic buck converter based on a mixed time frequency domain iteration is presented. Main parameters of this model are identified and wave propagation effects in the inductance pipe of the converter are investigated by simulation.

NOMENCLATURE

Δp pressure drop
 \mathbf{e} residual vector
 f_S switching frequency
 $G(s)$ transfer function
 \mathbf{I} identity matrix

j imaginary unit
 J_0, J_2 First kind Bessel functions of zero, resp., second order
 K bulk modulus of the fluid
 κ duty ratio
 κ polytropic exponent
 l length
 N number of samples
 ν kinematic viscosity of the fluid
 ω angular frequency
 p, p_N pressure, resp., nominal pressure drop
 q, Q_N flow rate, resp., nominal flow rate
 r radius
 ρ fluid density
 s laplacian variable
 t time
 T_P periodic time
 V volume
 ξ position
 \mathbf{z} parameter vector

INTRODUCTION

In digital hydraulic systems proportional or servo valves, which are sensitive against oil contamination, are replaced by cheap and robust digital on/off valves. One possibility is to realize hydraulic digital/analog converters by a parallel arrangement of digital valves with different nominal flow rates as proposed, for instance, in [1, 2]. Another approach is an operation of the

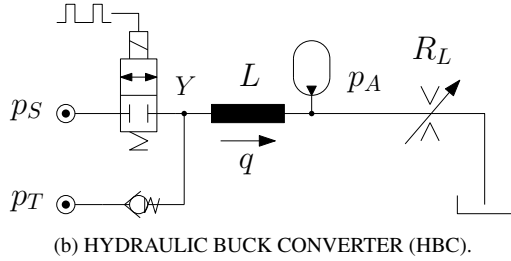
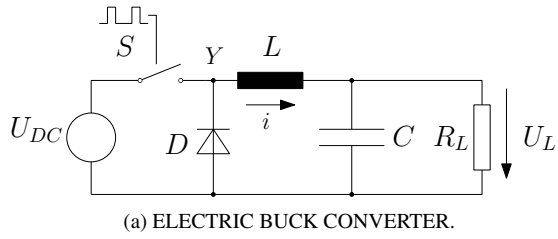
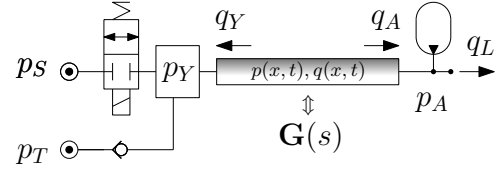


FIGURE 1: STEP DOWN CONVERTERS.

digital valves in pulse-width mode at a constant switching frequency according to [3,4]. Both methods represent a type of resistance control realized by switching valves, however, without any efficiency advantage. This drawback can be overcome by the use of hydraulic switching converters, which enable a significant increase of efficiency of hydraulic drive systems [5,6,7,8]. A simple switching converter is the Hydraulic Buck Converter (HBC), which is a concept transferred from power electronics to hydraulics as shown in Fig. 1. Both, in electronics and hydraulics, the buck converter represents a PWM controlled step down concept, which means, that the output voltage/pressure is always lower than the input voltage/pressure. In contrast to resistance control this concept allows a high efficiency even at working points with low output pressure control. The converters operate preferably at a constant switching frequency in pulse width mode. Today, the switching in hydraulics takes place in the range of 100Hz . Therefore, the switching valves must have a response time in the range of 1ms in order to realize a proper pulse-width. In contrast to motor converters (see e.g. [9]), where a flywheel at the shaft of a hydraulic motor is used as an inductance, the HBC exploits the inertia of the fluid in a simple inductance pipe, which allows a cost effective realization. At the output of the converter a hydraulic accumulator is located in order to attenuate the pressure fluctuations due to switching. For the basic design of an HBC a simple lumped parameter model is sufficient, which is not treated in this work. However, the nonlinear characteristics of some components and, furthermore, wave propagation effects in the main inductance cause some deviations to the theoretic characteristics. Moreover, pipe resonances can influence the system behavior. In this paper wave propagation effects in the main inductance are investigated. For this purpose, an ad-



vanced dynamic model of the HBC accounting for wave propagation effects is presented. The system parameters of a real HBC are identified. Using a combined mixed time-frequency domain iteration the system behavior is analyzed.

MODELING

The model of the HBC used for the investigations in this paper comprises the size and dynamics of the switching valves, wave propagation in the main inductance and the nonlinear gas spring of the pressure attenuator at the output of the converter. Furthermore, the dead volume in the node point Y resulting from dead end bores in the valve block is taken into account. The schematic of the investigated system is depicted in Fig. 2. In the following the individual model equations and the complete HBC model are presented.

The Orifice Equation. The commonly used square root characteristic of a flow through a valve orifice violates the Lipschitz criterion (see e.g. [10]), which is necessary for the existence and uniqueness of the solution of a differential equation. For this reason the flow through a valve orifice the model

$$q = \frac{Q_N}{\sqrt{p_N}} \sqrt[3]{\Delta p}, \quad (1)$$

with the nominal flow rate Q_N at the nominal pressure drop p_N and with the *orifice-root-function*

$$\sqrt[3]{\Delta p} = \begin{cases} -\sqrt{|\Delta p|} & \Delta p \leq -\Gamma \\ \frac{1}{2}\sqrt{\Gamma} \left(\frac{3\Delta p}{\Gamma} + \frac{(\Delta p)^2}{\Gamma^2} \right) & -\Gamma < \Delta p < 0 \\ 0 & \Delta p = 0 \\ \frac{1}{2}\sqrt{\Gamma} \left(\frac{3\Delta p}{\Gamma} - \frac{(\Delta p)^2}{\Gamma^2} \right) & 0 < \Delta p < \Gamma \\ \sqrt{\Delta p} & \Delta p \geq \Gamma \end{cases} \quad (2)$$

is employed based on [11]. In this model the square root characteristic is approximated by a polynomial within a certain interval around the origin of Δp with a limited slope to fulfill the Lipschitz condition. Compared to common pressure drops at hydraulic valves the coefficient Γ is very small and, thus, the square

root behavior is dominating. Equation (1) allows a flow in both directions.

Accumulator Model. To keep the equations simple also a simple model of the pressure attenuator at the output of the converter is desired. According to [12] the model

$$\frac{dp}{dt} = \frac{p^\kappa}{V_A \left(\frac{p_{0G}}{p}\right)^{\frac{1}{\kappa}}} q_{in} \quad (3)$$

can be used with the pressure p , the input flow rate q_{in} , the accumulator volume V_A , the gas pre-pressure p_{0G} and the polytropic exponent κ . This model assumes, that no resistance at the inlet of the accumulator is present, which is essential for a good pressure attenuation.

Pipe Model. For the converter model a laminar pipe flow and a linear material law are assumed in the main inductance. According to [13, 14] the effect of wave propagation and the frequency dependent friction in a straight pipe with a circular cross-section are described by transfer functions in frequency domain as follows

$$\begin{bmatrix} \hat{q}_0(s) \\ \hat{q}_1(s) \end{bmatrix} = \begin{bmatrix} \frac{1}{Z(s) \tanh(\gamma(s)l_p)} & -\frac{1}{Z(s) \sinh(\gamma(s)l_p)} \\ -\frac{1}{Z(s) \sinh(\gamma(s)l_p)} & \frac{1}{Z(s) \tanh(\gamma(s)l_p)} \end{bmatrix} \begin{bmatrix} \hat{p}_0(s) \\ \hat{p}_1(s) \end{bmatrix}, \quad (4)$$

with $Z(s) = \frac{\sqrt{K'p}}{r_p^2 \pi} \sqrt{-\frac{J_0(r^*)}{J_2(r^*)}}$, $\gamma(s) = \frac{s}{\sqrt{E'p}} \sqrt{-\frac{J_0(r^*)}{J_2(r^*)}}$, $r^* = j \sqrt{\frac{s}{v}} r_p$

and, j as the imaginary unit. The geometrical dimensions of the pipe are the pipe radius r_p and the pipe length l_p . This model is only valid, if all assumptions of a laminar pipe flow and a constant compression modulus are fulfilled.

The Hydraulic Buck Converter Model. With the individual models for valve flow, pressure build up in an accumulator and for linear wave propagation presented above the complete model of the HBC can be formulated. According to Fig. 2 the pressure build up equations in the node volume V_Y at the inductance pipe entrance and the accumulator V_A read

$$\dot{p}_Y \frac{V_Y}{K_{oil}} = q_Y + q_S + q_T \quad (5)$$

$$\dot{p}_A \frac{V_A \left(\frac{p_{0G}}{p_A}\right)^{\frac{1}{\kappa}}}{p_A \kappa} = q_A - q_L \quad (6)$$

with the flow rate

$$q_S = \text{sgI}(\xi_s(\kappa, t)) \frac{Q_{N_S}}{\sqrt{p_{N_S}}} \sqrt[3]{p_S - p_Y} \quad (7)$$

through the high pressure valve. In Eq. (7) the function

$$\text{sgI}(x) = \begin{cases} 0 & x \leq 0 \\ x & x > 0 \end{cases} \quad (8)$$

is used to describe the valve overlap of the spool valve, i.e., only a positive valve opening occurs according to a spool displacement like

$$\xi_s(\kappa, t) = \left(\frac{1}{2} + \frac{o_V}{100}\right) \left(\tanh\left(\frac{2\pi(t-t_{off})}{t_r}\right) - \tanh\left(\frac{2\pi(t-t_{off}-\kappa T_P)}{t_f}\right)\right) - 2\frac{o_V}{100}. \quad (9)$$

In Eq. (9) the parameters t_r and t_f denote the rise and the fall time of the valves. The valve overlap o_V is expressed in a percentage of the full spool stroke. The input of this spool model is the duty ratio κ according to the PWM control of the valve spool with respect to the cycle time T_P . The mechanical movement of the spool is modeled by two complementary and staggered \tanh -functions, where $0 < \xi_s < 1$ defines a hydraulic metering of the orifice. At $\xi_s = 1$ the valve is fully open. Negative values of ξ_s describe a movement behind the valve overlap. Since this case is hydraulically not relevant it is disregarded by Eq. (8). For identification reasons a time shift of the pulse along the cycle time interval can be realized with the variable t_{off} . An exemplary spool movement is illustrated in Fig. 3 for a certain parameter set and a duty ratio of $\kappa = 25\%$. The active switching valve has a nominal flow rate Q_{N_S} at a nominal pressure drop p_{N_S} . In the same manner, the flow rate through the tank sided check valve reads

$$q_T = \frac{Q_{N_C}}{\sqrt{p_{N_C}}} \text{sgI}\left(\sqrt[3]{p_T - p_Y}\right). \quad (10)$$

For simplicity, in Eq. (10) the response dynamics of the check valve is not considered, which is valid for check valves with sufficiently low opening pressure and much faster dynamics than the active switching valve.

Equation (5) and Eq. (6) represent the pressure dynamics at both ends of the inductance pipe in time domain. Due to the transcendental nature of the transfer function (Eq. (4)) no calculation

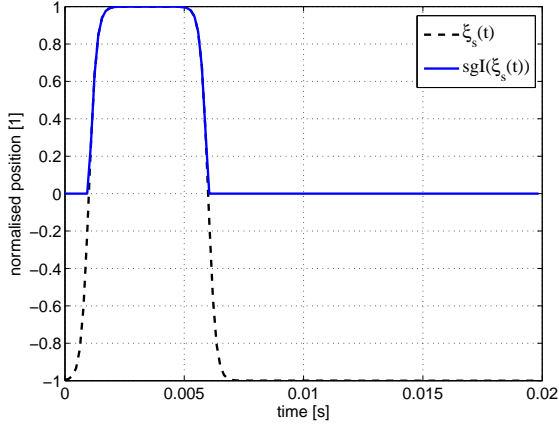


FIGURE 3: SPOOL MOVEMENT OF THE VALVE.

of the fluid dynamics in time domain is possible, hence, numerical methods have to be applied. The Fast-Fourier-Transformation (FFT) is an efficient method for periodic processes, which is the case in a steady state operating point of the HBC. Thus, the system response due to wave propagation effects in time domain can be efficiently calculated by Eq. (4) in combination with the Inverse-Fast-Fourier-Transformation (IFFT).

MIXED TIME-FREQUENCY DOMAIN ITERATION

The HBC model presented above consists of two nonlinear pressure build up equations and the linear transfer function in frequency domain accounting for wave propagation. Since a nonlinear system cannot be solved in frequency domain a combined method for simulation is required. Therefore, a combined mixed time-frequency domain iteration (TFDI) according to [15, 16, 17] is used in this paper. In the following, the basic idea of the TFDI will be outlined by its application to the dynamic model of the HBC according to Fig. 2. The two dynamic pressure states p_Y and p_A in time domain are considered in a certain periodic operating point of the HBC at constant duty ratio κ and the load flow rate q_L . Thus, Eqs. (5) and (6) can be written in the following form

$$\begin{bmatrix} \dot{p}_Y \\ \dot{p}_A \end{bmatrix} = \mathbf{f}(p_Y, p_A, \kappa, q_L). \quad (11)$$

Both pressure states are coupled by the main inductance of the converter, which is modeled in frequency domain according to Eq. (4). Due to the periodicity of the switching process, the solution of system (11) can be described in the following way

$$p_i(t) = a_{0,i} + \sum_{k=1}^{\infty} \{a_{k,i} \cos(k\omega_0 t) + b_{k,i} \sin(k\omega_0 t)\}, \quad (12)$$

with $\omega_0 = \frac{2\pi}{T_P}$ and the indices $i = A, Y$, which indicate the different ends of the pipe inductance according to Fig. 2. The time interval is given by $T_P = \frac{1}{f_S}$. For a numeric simulation, the continuous time interval $[0, T_P]$ is sampled at a constant sampling time T_S , with $\frac{T_P}{T_S} = N \in \mathbb{N}^+$ with N equidistant samples. Since the solution (12) is valid for every point in time, it is also valid at each sample point, which leads to the numeric periodic solution vector in time domain

$$\begin{bmatrix} \mathbf{p}_Y \\ \mathbf{p}_A \end{bmatrix} = [p_{Y,0}, \dots, p_{Y,N-1}, p_{A,0}, \dots, p_{A,N-1}]^T \quad (13)$$

of dimension $2N$. Due to this discretization and the periodicity both solutions for the pressure states read

$$p_i(t) = a_{0,i} + \sum_{k=1}^{\frac{N-1}{2}} \{a_{k,i} \cos(k\omega_0 t) + b_{k,i} \sin(k\omega_0 t)\} \quad (14)$$

with $i = A, Y$. The $2N$ real valued coefficients¹ $a_{0,i}$, $a_{k,i}$ and $b_{k,i}$ represent the pressure offset, the real- and the imaginary-part of the spectral components in frequency domain. This means, that the solution is well defined in both calculation domains. Thus, the solution in time domain can be easily transformed to frequency domain by the Fast-Fourier-Transformation (FFT). In accordance with Fig. 2, the dynamic time domain pressures p_Y and p_A at both ends of the main inductance can be transformed to their frequency domain representatives \hat{p}_Y and \hat{p}_A . Applying the pipe model of Eq. (4) the flow rates \hat{q}_Y and \hat{q}_A are calculated in frequency domain. The transformation back to time domain is carried out by the Inverse-Fast-Fourier-Transformation. In this way, wave propagation in the main inductance is taken into account.

The left hand side of Eq. (11), i.e., the derivatives of the pressure states with respect to time are approximated by means of a differential quotient in time domain, which is valid for a proper discretization of the problem. The pressure states can be written as vectors \mathbf{p}_Y and \mathbf{p}_A , consisting each of N unknowns, respectively. Hence, the problem for the analysis of one periodic cycle in time domain and at a certain operating point (κ, q_L) results in $2N$ equations for $2N$ unknowns

$$\mathbf{F}(\mathbf{p}_A, \mathbf{p}_Y) = \mathbf{0}, \quad (15)$$

which can be solved by established iteration algorithms.

¹In the considered case of Eq. (14) N is uneven. If N is an even number, then $b_{\frac{N}{2},i}$ is zero.

Detailed Formulation

The T_P -periodic solutions of system (11) are defined on the discretized time interval

$$\mathbf{t} = \frac{T_P}{N} [0, 1, \dots, N-1]^T \quad (16)$$

with $N \in \{2k-1 | k \in \mathbb{N}^+\}$ as the number of samples per switching period. The uneven number of samples is not restricted in general, but was chosen in this work for implementation reasons. However, for the desired resolution of the considered dynamic process, N is determined by Nyquist's criterion $\omega_{max} = \frac{\pi}{T_S} = \frac{N\pi}{T_P}$. In time domain the pressure states on the time interval according to Eq. (16) read

$$\mathbf{p}_Y = p_Y(\mathbf{t}) = [p_{Y,0}, \dots, p_{Y,N-1}]^T, \text{ with } p_{Y,0} = p_{Y,N} \quad (17)$$

and

$$\mathbf{p}_A = p_A(\mathbf{t}) = [p_{A,0}, \dots, p_{A,N-1}]^T, \text{ with } p_{A,0} = p_{A,N}. \quad (18)$$

The set of nonlinear equations for the iteration process according to Eq. (15) has the following form

$$\mathbf{e}(\mathbf{p}_Y, \mathbf{p}_A) = \begin{bmatrix} \mathbf{e}_{p_Y} \\ \mathbf{e}_{p_A} \end{bmatrix} \stackrel{!}{=} \mathbf{0}, \quad (19)$$

where \mathbf{e}_{p_Y} and \mathbf{e}_{p_A} stand for the residual vectors of the discretized equations (5) and (6), respectively. They read

$$\mathbf{e}_{p_Y} = -\frac{V_Y}{K_{oil}} \frac{\Delta \mathbf{p}_Y}{\Delta t} + (\mathbf{q}_Y + \mathbf{q}_S + \mathbf{q}_T) \quad (20)$$

and

$$\mathbf{e}_{p_A} = -\frac{V_A p_{0G}^{\frac{1}{\kappa}}}{\kappa} \text{diag}\{\mathbf{p}_A\}^{-\frac{\kappa+1}{\kappa}} \frac{\Delta \mathbf{p}_A}{\Delta t} + (\mathbf{q}_A - \mathbf{q}_L) \quad (21)$$

under the assumption of $p_A \geq p_{0G} > 0$ for every sampling point within the considered time interval. The derivatives with respect to time of the periodic pressure vectors are approximated by the central differential quotient

$$\frac{\Delta \mathbf{p}_i}{\Delta t} = \frac{1}{2T_S} \left(\begin{bmatrix} p_{i,1} \\ \vdots \\ p_{i,N-1} \\ p_{i,0} \end{bmatrix} - \begin{bmatrix} p_{i,N-1} \\ p_{i,0} \\ \vdots \\ p_{i,N-2} \end{bmatrix} \right) = \frac{1}{2T_S} (\mathbf{T}_{SH} - \mathbf{T}_{SH}^T) \mathbf{p}_i \quad (22)$$

with $i = A, Y$, the sampling time T_S and the shifting matrix

$$\mathbf{T}_{SH} = \begin{bmatrix} \mathbf{0} & \mathbf{I} \\ \mathbf{1} & \mathbf{0} \end{bmatrix}. \quad (23)$$

The flow rate vector of the active switching valve reads

$$\mathbf{q}_S = \frac{Q_{N_S}}{\sqrt{p_{N_S}}} \text{diag}\{\text{sgI}(\xi_s(\mathbf{t}))\} \sqrt[p_S - p_Y]{} \quad (24)$$

and the flow rate vector of the check valve follows to

$$\mathbf{q}_T = \frac{Q_{N_{CV}}}{\sqrt{p_{N_{CV}}}} \text{sgI}\left(\sqrt[p_T - p_Y]{}\right). \quad (25)$$

The flow rate vectors \mathbf{q}_Y and \mathbf{q}_A at the different pipe ends are calculated in frequency domain. Assuming periodicity of the switching process, with $G_{ik}(j\omega)$, $i, k = 1, 2$ regarding to Eq. (4) and using the Fourier transformation $\hat{p}_i(j\omega) = \mathcal{F}\{p_i(t)\}$ with $i = A, Y$, the dynamic flow rates calculate to

$$\begin{bmatrix} \hat{q}_Y(j\omega) \\ \hat{q}_A(j\omega) \end{bmatrix} = \begin{bmatrix} G_{11}(j\omega) & G_{12}(j\omega) \\ G_{21}(j\omega) & G_{22}(j\omega) \end{bmatrix} \begin{bmatrix} \hat{p}_Y(j\omega) \\ \hat{p}_A(j\omega) \end{bmatrix}. \quad (26)$$

Applying the inverse Fourier transformation the flow rates in time domain read $q_i(t) = \mathcal{F}^{-1}\{q_i(j\omega)\}$, $i = A, Y$. Considering the periodicity on the discretized time interval the Fourier transform corresponds to the Discrete Fourier Transform (DFT) and its inverse, respectively. The numeric implementation of the DFT in *Matlab*TM is also called Fast-Fourier-Transform and Inverse-Fast-Fourier-Transform, respectively. Thus, the flow rate vectors at both ends of the inductance pipe in time domain calculate to

$$\mathbf{q}_Y = \text{ifft}\{\mathbf{G}_{11}(j\omega) \text{fft}\{\mathbf{p}_Y\} + \mathbf{G}_{12}(j\omega) \text{fft}\{\mathbf{p}_A\}\} \quad (27)$$

$$\mathbf{q}_A = \text{ifft}\{\mathbf{G}_{21}(j\omega) \text{fft}\{\mathbf{p}_Y\} + \mathbf{G}_{22}(j\omega) \text{fft}\{\mathbf{p}_A\}\}, \quad (28)$$

where the transfer functions $G_{ik}(j\omega)$, $i, k = 1, 2$ of Eq. (26) are replaced by the discretized transfer matrices

$$\mathbf{G}_{ik}(j\omega) = \text{diag}\{G_{ik}(j\omega)\}, \quad i, k = 1, 2 \quad (29)$$

accounting for wave propagation. The vector of the discrete angular frequencies reads

$$\omega = \omega_0 \left[0, 1, 2, \dots, \frac{N-1}{2}, \frac{N-1}{2}, \frac{1-N}{2} + 1, \frac{1-N}{2} + 2, \dots, -1 \right] \quad (30)$$

with $\omega_0 = \frac{2\pi}{T_p}$. The load flow rate vector \mathbf{q}_L in Eq. (21) represents an input vector, which must be a periodic signal. In the considered case it is sufficient to use a constant load flow rate $\mathbf{q}_L = q_L [1, \dots, 1]^T$ with a constant factor q_L .

Since the discretized equations (20) and (21) are nonlinear, the problem must be solved iteratively by appropriate algorithms, for instance, by *fsolve* in *Matlab*TM. The convergence of such iteration algorithms depends, besides other specific parameters, strongly on the initial conditions \mathbf{p}_{Y_0} and \mathbf{p}_{A_0} . In the selected simulation cases, the choice

$$\mathbf{p}_{i_0} = \frac{p_S + p_T}{2} [1, \dots, 1]^T, \quad i = A, Y \quad (31)$$

yielded always physically reasonable results. However, the uniqueness of the obtained solution is not yet studied. In view of the nonlinearities, particularly of the accumulator, multiple solutions might exist.

Improvement of the Calculation Performance

Many iteration techniques are based on Newton's method, which needs information about Jacobian matrix. The Jacobian is often approximated by numerical differentiation, which needs a large number of function calls. This can be avoided by evaluating the Jacobian matrix of Eq. (19), which reads in the considered case

$$\mathbf{J} = \begin{bmatrix} \frac{\partial}{\partial \mathbf{p}_Y} \mathbf{e}_{p_Y} & \frac{\partial}{\partial \mathbf{p}_A} \mathbf{q}_Y \\ \frac{\partial}{\partial \mathbf{p}_Y} \mathbf{q}_A & \frac{\partial}{\partial \mathbf{p}_A} \mathbf{e}_{p_A} \end{bmatrix} \quad (32)$$

with

$$\begin{aligned} \frac{\partial}{\partial \mathbf{p}_Y} \mathbf{e}_{p_Y} &= -\frac{\partial}{\partial \mathbf{p}_Y} \left(\frac{\Delta \mathbf{p}_Y}{\Delta t} \right) \frac{V_Y}{K_{oil}} + \\ &+ \frac{\partial}{\partial \mathbf{p}_Y} (\mathbf{q}_{VS} + \mathbf{q}_{CT}) + \frac{\partial}{\partial \mathbf{p}_Y} \mathbf{q}_Y \end{aligned} \quad (33)$$

$$\begin{aligned} \frac{\partial}{\partial \mathbf{p}_A} \mathbf{e}_{p_A} &= -\frac{V_A p_{0G}^{\frac{1}{\kappa}}}{\kappa} \text{diag} \{ \mathbf{p}_A \}^{-\frac{\kappa+1}{\kappa}} \frac{\partial}{\partial \mathbf{p}_A} \left(\frac{\Delta \mathbf{p}_A}{\Delta t} \right) + \frac{\partial}{\partial \mathbf{p}_A} \mathbf{q}_A + \\ &+ \frac{V_A p_{0G}^{\frac{1}{\kappa}}}{\kappa} \left(1 + \frac{1}{\kappa} \right) \text{diag} \{ \mathbf{p}_A \}^{-\frac{2\kappa+1}{\kappa}} \text{diag} \left\{ \frac{\Delta \mathbf{p}_A}{\Delta t} \right\} \end{aligned} \quad (34)$$

and

$$\frac{\partial}{\partial p_i} \left(\frac{\Delta \mathbf{p}_i}{\Delta t} \right) = \frac{1}{2T_S} (\mathbf{T}_{SH} - \mathbf{T}_{SH}^T). \quad (35)$$

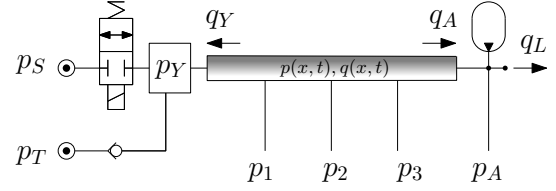


FIGURE 4: PRESSURE MEASUREMENTS.

The influence of the different pressure states on the corresponding flow rates at both ends of the pipe inductance read

$$\frac{\partial}{\partial \mathbf{p}_Y} \mathbf{q}_Y = \text{ifft} \{ \mathbf{G}_{11}(j\omega) \text{fft} \{ \mathbf{I} \} \} \quad (36)$$

$$\frac{\partial}{\partial \mathbf{p}_A} \mathbf{q}_Y = \text{ifft} \{ \mathbf{G}_{12}(j\omega) \text{fft} \{ \mathbf{I} \} \} \quad (37)$$

$$\frac{\partial}{\partial \mathbf{p}_Y} \mathbf{q}_A = \text{ifft} \{ \mathbf{G}_{21}(j\omega) \text{fft} \{ \mathbf{I} \} \} \quad (38)$$

$$\frac{\partial}{\partial \mathbf{p}_A} \mathbf{q}_A = \text{ifft} \{ \mathbf{G}_{22}(j\omega) \text{fft} \{ \mathbf{I} \} \}. \quad (39)$$

Providing the Jacobian matrix (32) to the used iteration algorithm *fsolve* in *Matlab*TM reduces the calculation time ¹/₁₅.

IDENTIFICATION

For identification a configuration according to Fig. 4 is considered. Along the main inductance pipe several pressure transducers were installed to evaluate the pressure responses on different locations of the inductance pipe. These measurements are compared to the TFDI calculations with the simulation model. The real measuring configuration of the HBC according to Fig. 4 is depicted in Fig. 5. The parameter identification was carried out by an optimization process using the routine *lsqnonlin* of *Matlab*TM. This algorithm solves nonlinear least squares curve fitting problems of the form

$$\min_{\mathbf{z}} \|\mathbf{e}(\mathbf{z})\|_2^2 = \min_{\mathbf{z}} (e_1(\mathbf{z})^2 + e_2(\mathbf{z})^2 + \dots + e_N(\mathbf{z})^2) \quad (40)$$

with the residual vector \mathbf{e} and the parameter vector \mathbf{z} . The residual vector \mathbf{e} represents the difference between the measured periodic pressure responses and the corresponding response calculated with the TFDI according to Fig. 4. The vector \mathbf{z} contains the parameters to be identified. The iteration process starts with appropriate initial values \mathbf{z}_0 and the algorithm finds a minimum of the sum of squares of the components of \mathbf{e} according to Eq. (40). To obtain physically meaningful results upper and lower bounds of the individual parameters of \mathbf{z} were defined.

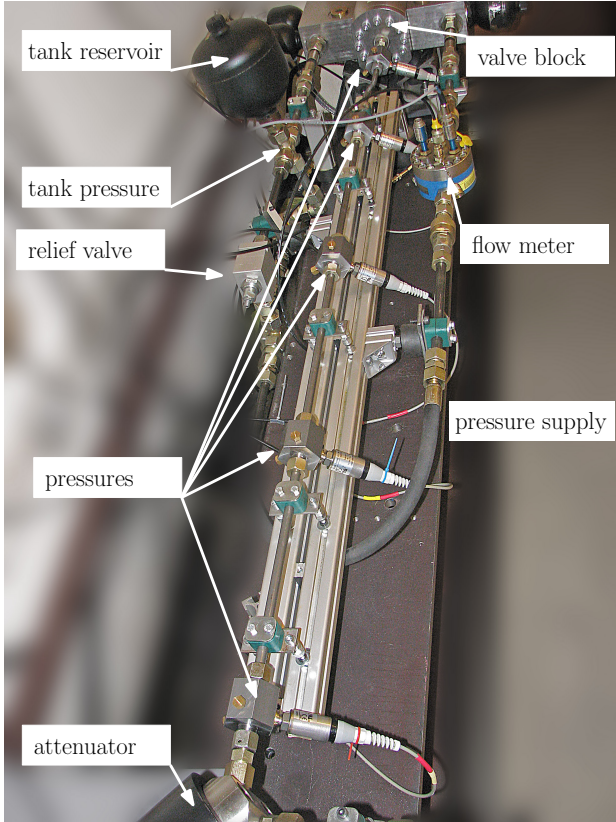


FIGURE 5: THE TEST RIG.

In the concrete case the HBC prototype of Fig. 5 was operated at a switching frequency of 30Hz and was supplied with a system pressure of $p_S = 150\text{bar}$ and a tank pressure of $p_T = 10\text{bar}$. As an operating point at a duty ratio of $\kappa = 20\%$ and a load flow rate of $q_L = 17.5 \frac{l}{min}$ was chosen. The result of this parameter identification is depicted in Fig. 6, where the thick lines represent the measured pressure response and the thinner lines the simulation results. In the lower diagram the residuals at the end of the optimization process is depicted. The identified parameters of the optimization process are listed with the corresponding real values in Tab. 1. It must be remarked, that not all real parameters, like for instance the effective bulk modulus or the viscosity of the fluid, were known a priori. Furthermore, no measurement of the spool position of the switching valve was available, thus the time offset t_{off} and the correction of κ were determined by the parameter optimization. The deviation between some identified parameters to the real values are also physically plausible. For instance, the identified nominal flow rates of the switching valve and the check valve are lower than the supposed real values, which is realistic since the flow channels of the valve block result in additional resistances. Also the higher identified viscosity shows that more damping is present

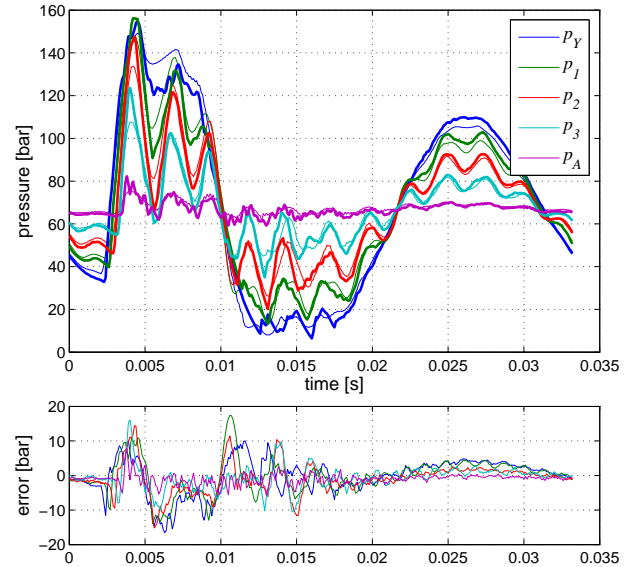


FIGURE 6: IDENTIFICATION RESULTS.

TABLE 1: IDENTIFIED PARAMETERS.

Parameter	Identified values \mathbf{z}	Real values \mathbf{z}_{real}
pipe length	$l_p = 1.714\text{ m}$	$l_{p_r} = 1.7\text{ m}$
bulk modulus	$K_{oil} = 15176\text{ bar}$	$K_{oil_r} = ?\text{ bar}$
first pipe element	$l_m = 0.145\text{ m}$	$l_{m_r} = 0.1\text{ m}$
node volume	$V_Y = 0.385\text{ l}$	$V_{Y_r} \approx 0.25\text{ l}$
oil viscosity	$\nu = 58.63\text{ cSt}$	$\nu_r \approx 46\text{ cSt}$
nominal flow rate switching valve @5bar	$Q_{N_S} = 37.338 \frac{l}{min}$	$Q_{N_{S_r}} \approx 45 \frac{l}{min}$
nominal flow rate check valve @5bar	$Q_{N_C} = 49.715 \frac{l}{min}$	$Q_{N_{C_r}} \approx 120 \frac{l}{min}$
attenuator pre-pressure	$p_G = 29.28\text{ bar}$	$p_{G_r} \approx 40\text{ bar}$
time offset	$t_{off} = 2.112\text{ ms}$	$t_{off_r} = ?\text{ ms}$
correction of κ	$\Delta_\kappa = -0.42\%$	$\Delta_{\kappa_r} = ?\%$

TABLE 2: HBC SIMULATION PARAMETERS.

Parameter	Value
supply pressure	$p_S = 150 \text{ bar}$
tank pressure	$p_T = 10 \text{ bar}$
bulk modulus of the fluid	$K_{oil} = 14000 \text{ bar}$
density of the fluid	$\rho_{oil} = 860 \frac{\text{kg}}{\text{m}^3}$
viscosity of the fluid	$\nu = 46 \frac{\text{mm}^2}{\text{s}}$
switching valve	$Q_{N_S} = 45 \frac{\text{l}}{\text{min}} @ 5 \text{ bar}$
check valve	$Q_{N_T} = 120 \frac{\text{l}}{\text{min}} @ 5 \text{ bar}$
switching time	$t_r = t_f = 2 \text{ ms}$
valve covering	$c_V = 50\%$
switching frequency	$f_S = 50 \text{ Hz}$
length of inductance pipe	$l_p = 1.7 \text{ m}$
diameter of inductance pipe	$d_p = 8 \text{ mm}$
volume of the accumulator	$V_A = 0.32 \text{ l}$
pre-pressure of accumulator	$p_{0G} = 20 \text{ bar}$
polytropic exponent	$\kappa = 1.3$

in the system than in the simulation model. Hence, the system parameters identified with the presented method are reasonable.

SIMULATION

Based on the satisfying identification results a comprehensive simulation study was carried out. Its main purpose was to classify the influence of certain system parameters on the performance characteristics of the HBC. The numeric simulation parameters of the HBC used for the following simulations are listed in Tab. 2, which correspond to a real HBC prototype. Previous investigations (see for instance [12]) taught, that besides other dissipative effects the capacitance in the node point Y of the HBC has a significant influence on the efficiency. In fact, a larger node capacitance causes also higher losses, because it must be charged and discharged at every switching cycle. Thus, with a smaller node volume a higher efficiency performance can be achieved because of lower charging losses. This is a mandate for the valve block design to minimize the channel volumes between the valves and the inductance pipe, which are creating substantial charging losses. Different values of the node capacitance were simulated to know about the impact of the HBC performance. All other system parameters were kept constant.

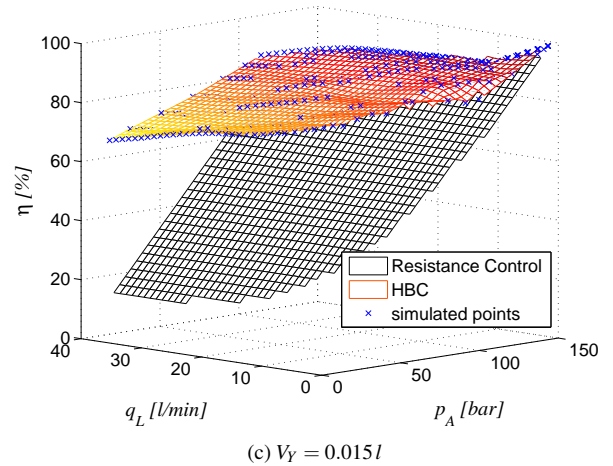
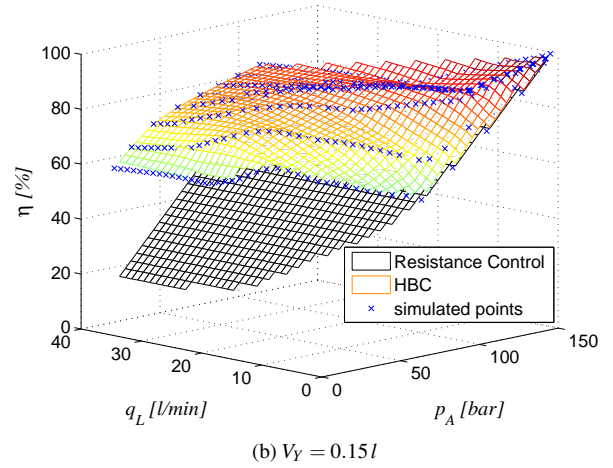
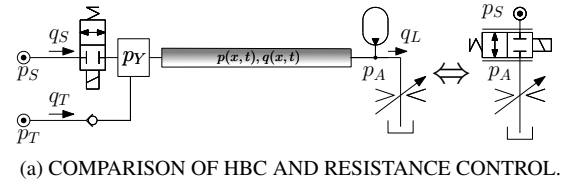


FIGURE 7: EFFICIENCY CHARACTERISTICS $\eta(q_L, p_A)$.

Converter Characteristics

A series of TFDI simulations was carried out for the calculation of the efficiency characteristics of an HBC with the parameters according to Tab. 2. The different working points were defined by the load flow rate $q_L = 0, \dots, 40 \frac{\text{l}}{\text{min}}$ and the duty ratio $\kappa = 0, \dots, 80\%$. In Fig. 7 the converter efficiency characteristics for two different node volumes are opposed. Regarding Fig. 7a

the efficiencies of the HBC and resistance control (RC) read

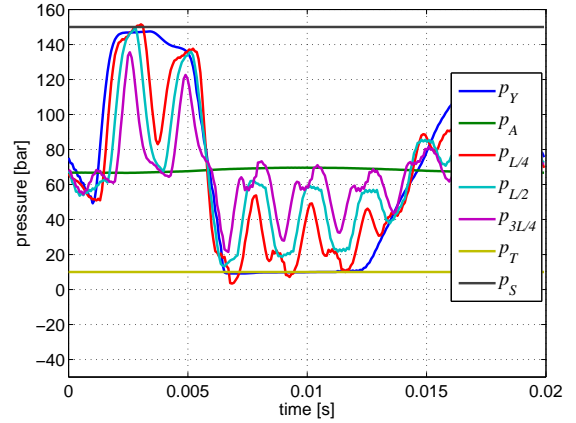
$$\eta_{HBC} = \frac{\int_0^{T_P} p_A q_L dt}{\int_0^{T_P} (p_S q_S + p_T q_T) dt} \text{ and } \eta_{RC} = \frac{p_A}{p_S}. \quad (41)$$

In Fig. 7b and Fig. 7c the markers represent the simulated working points of the HBC each calculated with an individual TFDI simulation. The lower meshed surface is the corresponding efficiency of a resistance control. Figure 7b represents the characteristics with a node volume of $V_Y = 0.15l$, and, Fig. 7c shows the results with a node volume $V_Y = 0.015l$. It can be seen, that the efficiency performance of the converter depends strongly on the size of this volume. A comparison of both figures makes clear, that with a smaller node volume a higher efficiency performance can be achieved over a wide operating range.

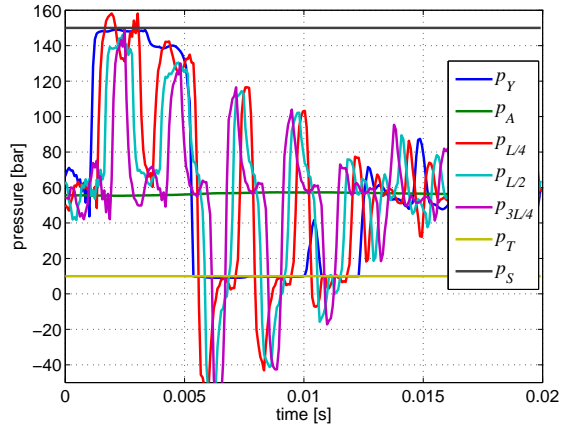
On the other hand, an analysis of selected pressure signals at different locations along the main inductance shows a remarkable resonance effect, which obviously depends strongly on the size of the node capacitance. The pressure signals in the main inductance were investigated at three equidistant locations between both ends of the main inductance pipe, like depicted in Fig. 4. The distributed pressure signals in a certain working point of the same HBC, but with different node volumes ($V_Y = 0.15l$ and $0.015l$) are illustrated in Fig. 8. In Fig. 8b - where the small node volume is considered - tremendous negative pressure values occur within the different pipe ends, while at the end of the pipe no cavitation appears. Of course, the negative amplitudes must not be interpreted as negative pressure levels, just the linear wave propagation model which does not account for cavitation leads to this result. Cavitation creates impact losses, bad noise and additional mechanical stress of the pipe. Obviously, the small node volume enables a sharp broad band excitation for the main inductance and, thus, pressure waves of very high magnitude are traveling through the pipe. Comparing both results of Fig. 8 the oscillations at the different locations show the same phase shift. Thus, this phenomenon represents the $\lambda/2$ -resonance of the inductance pipe as illustrated on top of Fig. 9. This resonance effect occurs at the second natural frequency

$$f_{\lambda/2} = \frac{c_0}{2L} \quad (42)$$

of the pipe, which is strictly determined by the length of the pipe line and the fluid parameters. In a proper designed HBC the $\lambda/2$ -resonance is usually much higher than the switching frequency, but the broad band excitation due to switching in combination with a small node volume provokes this resonance effect. A larger node volume filters the high frequency components of the switching process such that a strong excitation of the second natural frequency of the inductance pipe is prevented. In the design



(a) $V_Y = 0.15l$



(b) $V_Y = 0.015l$

FIGURE 8: DISTRIBUTED PRESSURE SIMULATIONS.

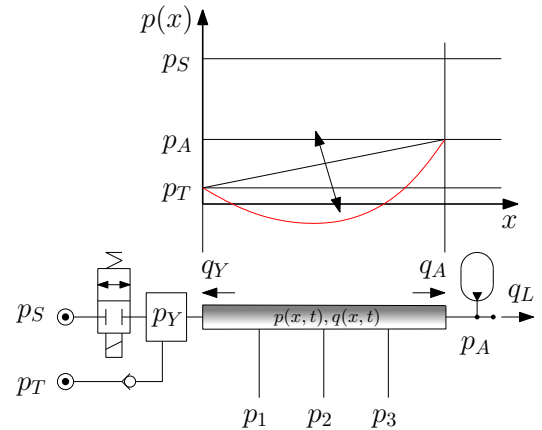


FIGURE 9: $\lambda/2$ -RESONANCE IN MAIN INDUCTANCE.

of an HBC the node volume size is a trade off on efficiency but preventing unwanted resonances in the inductance pipe.

SUMMARY AND OUTLOOK

In this paper the modeling, identification and simulation of an HBC including the analysis of wave propagation effects in the main inductance of the converter were presented. In the modeling process the components with a nonlinear behavior, like valves and the polytropic change of state in the gas spring of the attenuator, were considered in time domain. For the effect of linear wave propagation in the inductance pipe an established frequency domain model was used. A mixed time-frequency domain iteration was employed to solve the model equations for simulation. The identification results confirmed the validity of the mathematical model. On the one hand simulations taught, that a reduction of the capacitance in the node point increases the efficiency performance of the converter. On the other hand the small node capacitance leads to high frequency excitation in the inductance pipe due to the switching process, which may lead to cavitation in the inductance pipe. In fact, such a behavior could not be confirmed, because the simulation model did not consider the effect of cavitation. But it is clear, that cavitation should be avoided at all for durability and noise reasons.

For a proper simulation of cavitation effects in the main inductance pipe a qualified wave propagation model is necessary. Investigation in [18] showed, that in the low pressure range thermoelasticity and entrained air play an important role in the material behavior of hydraulic fluids, which must be accounted for in future simulations.

ACKNOWLEDGMENT

This work was sponsored by the Austrian Center of Competence in Mechatronics (ACCM) which is a COMET K2 center and is funded by the Austrian Federal Government, the Federal State Upper Austria and its Scientific Partners.

REFERENCES

- [1] Linjama, M., and Vilenius, M., 2007. "Digital Hydraulics - Towards Perfect Valve Technology". In Proceedings of The 10th Scandinavian International Conference on Fluid Power, SICFP'07, May 21-23, Tampere, Finland.
- [2] Linjama, M., 2008. "Digital Hydraulics Research at IHA". In Proceedings of The 1st Workshop on Digital Fluid Power, 3rd October, Tampere, Finland.
- [3] Hanxiu, L., Yuqing, Y., and Xuli, 1987. The PWM Electrohydraulic Control System Using A Computer. Tech. rep., Zhejiang University.
- [4] Winkler, B., Ladner, K., Kogler, H., and Scheidl, R., 2005. "Switching control of a linear hydraulic drive - experimental analysis". In Proceedings of the 9th Scandinavian International Conference on Fluid Power, Linköping, Sweden.
- [5] Brown, F. T., 1987. "Switched Reactance Hydraulics: A new way to control Fluid Power". In National Conference on Fluid Power, pp. 25-33.
- [6] Scheidl, R., Schindler, D., Riha, G., and Leitner, W., 1995. "Basics for the Energy-Efficient Control of Hydraulic Drives by Switching Techniques". In Proceedings of the 3rd Conference on Mechatronics and Robots, ISBN: 3-519-02625-2, J. Lückel, ed.
- [7] Scheidl, R., Garstener, M., and Grammer, S., 1996. "The Resonance Converter - A Novel Method for Hydraulic Fluid Power Control". In Proceedings of Mechatronics '96, Guimaraes, Portugal, ISBN: 972-8063-0.
- [8] Kogler, H., and Scheidl, R., 2008. "Two Basic Concepts of Hydraulic Switching Converters". In Proceedings of the First Workshop on Digital Fluid Power, DFP08, Tampere, Finland.
- [9] Wang, F., Gu, L., and Chen, Y., 2011. "A continuously variable hydraulic pressure converter based on high-speed on-off valves". *Mechatronics*, **21**(8), pp. 1298-1308.
- [10] Khalil, H. K., 1996. *Nonlinear Systems*. Prentice Hall.
- [11] Ellman, A. K., and Piche, R. A., 1996. "A modified orifice flow formula for numerical simulation". *Journal of Dynamic Systems, Measurement, and Control*, **121** (4), pp. 721-724.
- [12] Kogler, H., 2012. "The Hydraulic Buck Converter - Conceptual Study and Experiments". PhD thesis, Johannes Kepler University, Linz, Austria.
- [13] D'Souza, A. F., and Oldenburger, R., 1964. "Dynamic response of fluid lines". *Trans. ASME, J. Basic Engineering*, **86**, pp. 589-598.
- [14] Theissen, H., 1983. "Die Berücksichtigung instationärer Rohrströmung bei der Simulation hydraulischer Anlagen". PhD thesis, Rheinisch-Westfälische Technische Hochschule Aachen.
- [15] Cameron, T. M., and Griffin, J. H., 1989. "An alternating frequency/time domain method for calculating the steady-state response of nonlinear dynamic systems". *Journal of Applied Mechanics*, **56**, pp. 149-154.
- [16] Manhartgruber, B., Mikota, G., and Scheidl, R., 2005. "Modelling of a switching Control Hydraulic System". *Mathematical Computer Modelling of Dynamical Systems*, **11**(3), pp. 329-344.
- [17] Scheidl, R., Manhartgruber, B., and Kogler, H., 2011. "Mixed time-frequency domain simulation of a hydraulic inductance pipe with a check valve". *Proc. of the Institution of Mechanical Engineers, Part C: Journal of Mechanical Engineering Science*, **225**, pp. 2413-2421.
- [18] Haas, R., 2013. "Material behavior of hydraulic fluids under the influence of thermoelasticity and entrained air". PhD thesis, Johannes Kepler University, Linz.